Manuscript submitted to:

AIMS Energy

Volume 3, Issue 1, 101–120

DOI:10.3934/energy.2015.1.101

Received 6 November 2014, Accepted 28 January 2015, Published 26 February 2015

Research article

From local wind energy resource to national wind power production

Wolf-Gerrit Früh[1]*

[1] Institute of Mechanical, Process and Energy Engineering, School of Engineering and Physical Sciences, Heriot-Watt University, Riccarton, Edinburgh EH14 4AS, Scotland, UK

* **Correspondence:** w.g.fruh@hw.ac.uk; Tel: +44-131-451-4374; Fax: +44-131-451-3129

Abstract: Wind power is one of the most established renewable power resources yet it is also one of the most volatile resources. This poses a key challenge for successfully integrating wind power at a large scale into the power grid. Here we present an analysis of the time scales associated with wind power from hourly to seasonal fluctuations and how combining spatially distributed wind power sources helps to reduce its volatility. The analysis, based on observed wind speeds, is then generalised in a simple statistical model to develop a tool which can estimate the power output profile from a particular consortium of wind power sources. As the estimator only uses the local, or the mean national, wind resource and the mean distance between the sites to estimate the joint power output profile, it can be used by developers to estimate the reliability of their joint power output and to form the most effective consortium.

Keywords: wind energy resource, wind power production, regional aggregation, Virtual Power Plant

1. Introduction

With the global drive to increase the contribution of low-carbon renewable energy resources to power generation, wind energy is experiencing sustained and substantial growth in almost every part of the world. Wind power in particular is one of the key technologies as it is mature, able to be installed in utility-scale installations with installed capacities of hundreds of MW, and able to compete commercially with conventional generation, e.g. [10]. However, it is also a resource associated with a significant variability at virtually all time scales, from the duration of turbulent gusts, through daily and seasonal cycles, to long-term changes associated with climate change, where each time scale poses different challenges to integrating wind energy, e.g. [2], from power quality issues to reliability issues and strategic planning. Ultimately, the instantaneous demand and the consumption over a period must be balanced by the supply. To achieve this balance, a comprehensive portfolio of back-up generation, interconnection, demand management, and energy storage must be used.

The UK electricity grid is an ideal case study for the integration of variable renewable energy into the national transmission system, partly because it has a good resource in many areas and forms, from solar through wind to wave and tidal power but also because of the nature of the electricity grid. The UK is a sizeable industrialised island with a well-developed transmission and distribution network supplying a national demand of between 20 GW during summer off-peak and 60 GW during winter peak demand [26], yet with limited connection to the Irish and mainland European systems with a combined capacity of 4 GW in 2013 [25].

Much research has investigated the overall resource for specific sites, from land-based wind speed measurements [11, 15, 30, 37], satellite observations [33], or by using climate or numerical weather prediction models. [7], and statistical downscaling [8], or dynamic downscaling [27]. Equally, short-term wind speed and wind power prediction has been extensively researched, e.g. [14, 31].

A recent analysis of the variability characteristics of the main renewable energy resources for the UK [6] has provided detailed insight into the characteristics associated with a small set of locations but not addressed the issue what the result is when the variability from several locations is combined into a common transmission network. For other networks, it has been shown that regional aggregation of wind farms in Texas [21] or California [34] reduce in particular the high-frequency variability and that combining power from distant wind farms across the USA leads to substantial reduction in variability at all frequencies [13]. A highly idealised

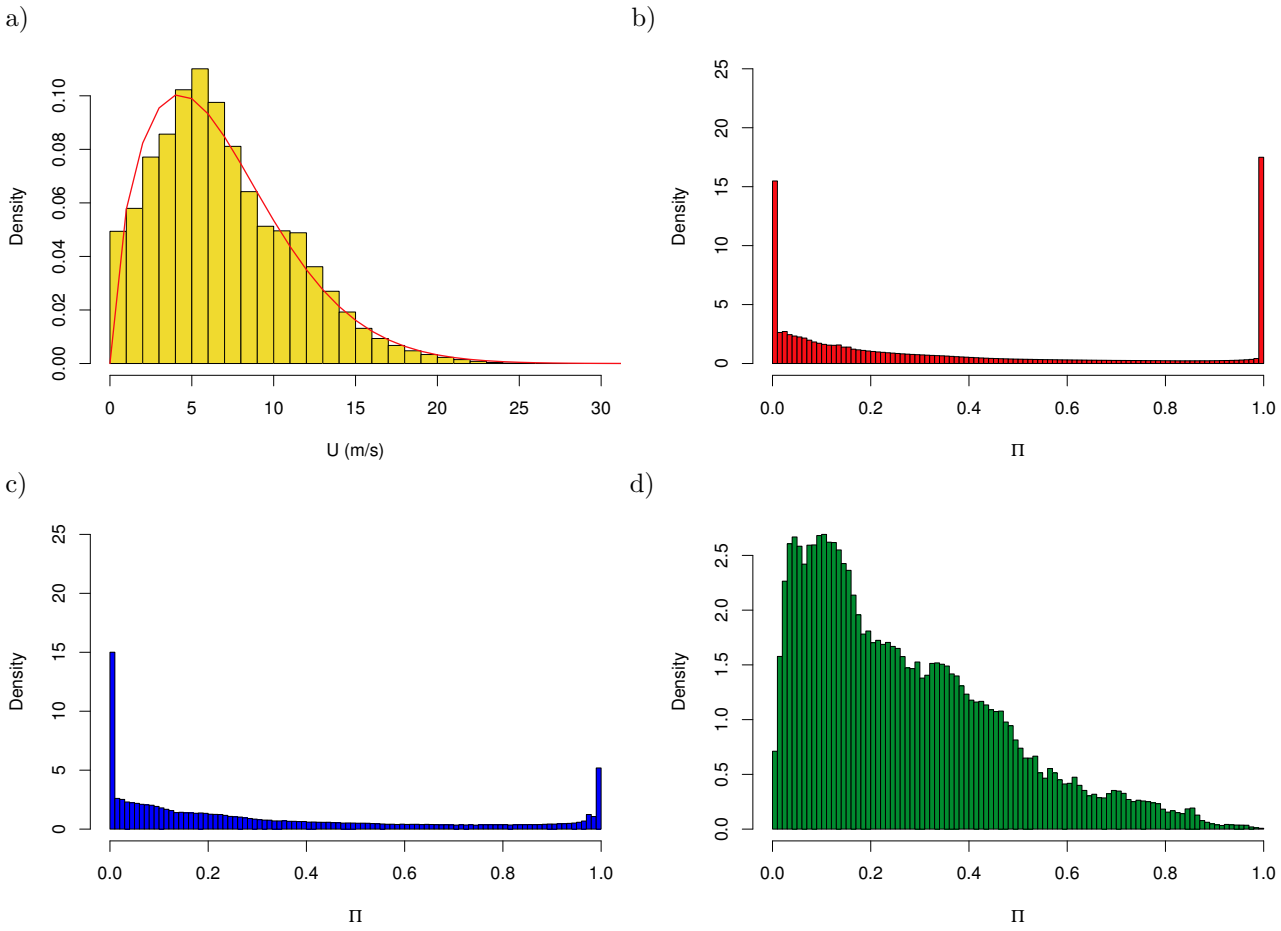

Figure 1. Illustration of the wind energy distribution and power distributions; a) wind speed histogram and best-fit Weibull curve; b) power output distribution from a single turbine divided by its rated power; c) same as b) but for a wind farm; d) distribution of wind power contribution to the UK's national transmission grid divided by the maximum wind power over that 2-year period.

analysis of meeting demand by 100% wind from a single site suggested that a large part of the required energy storage volume would be needed to cover time periods of less than 12 hours [17]. An open question is, how this would change if wind power from distant sites is combined.

The profile of the output from a single wind turbine, a wind farm and the full national fleet of wind farms is illustrated in Figure 1. Figure 1.a shows the wind speed distribution for a typical year of wind speed measurements at a representative site in the UK (where the number of hourly measurements have been rescaled to a probability density, referred to as 'Density' in the axis labels, such that the area under the histogram is equal to 1). Superimposed is the matching Weibull distribution, which is often used to describe wind speed statistics and which is formally defined in §2.2. Figure 1.b shows the distribution of the power output from a single wind turbine near that site and frame c) that from a wind farm. To compare the performance of a single turbine with that of a farm or a national fleet of wind farm, the power output is normalised against the combined capacity of the participating turbines. That means that the normalised power, Π, in Figure 1.b is the power output divided by the rated power of the turbine, $\Pi \equiv P/P_R$, while in Figure 1.c it is the power output from that wind farm divided by the installed capacity of that wind farm. Figure 1.d shows the distribution of the wind power fed into the UK transmission grid over the same period (data supplied from [26]). Figure 1.b shows that this particular turbine generated either nothing or at full rated power for about 15% or 20% of the year, respectively, and the majority of the remaining time the turbine generated between 1% and 30% of the installed capacity.

The extreme cases of no or full output are somewhat reduced in the case of a wind farm with turbines no more than a few kilometres apart. However, the result of combining all wind turbines across the entire UK covering a maximum distance between turbines of around 1000 km, the wind power profile is substantially different and much less extreme. Now the cases of either no output at all or the entire installed wind capacity generating at maximum are extremely rare, but the total wind power is well distributed for the vast majority of the time over a range from around 5% to 60% of the installed capacity. From a point of electricity produced over a year, all three cases shown here result in the same capacity factor or annual electricity production per installed capacity. However, for planning purposes of supplying power to the consumer, the profile shown in Figure 1.d is obviously much better because the actual output is frequently around the mean output, instead of frequently being at the extremes. This paper explores how the wind power production changes from the volatile behaviour of a single wind farm to a much more moderate behaviour as more and more wind farms contribute to the overall wind power over the area of a national transmission grid.

In this paper, the main focus is on the effect of regional and national wind power aggregation on the instantaneous power output and the power fluctuations. In addition, the effect of power aggregation on the longer time scales relevant for energy storage and planning of traditional generation will be also be discussed. The two key questions are: firstly, does wind power aggregation lead to making the availability of wind power more reliable and thereby mitigate the escalating need for alternative generation or energy storage and, secondly, do wind power fluctuations smooth each other out and thereby reduce the need for substantial alternative generation to respond at very short time scales above the current level of balancing operated by the transmission system operator?

To address these questions, the wind speed from a regional distribution of land-based anemometers will be used to estimate wind power which is then aggregated incrementally over the area of the mainland UK. To generalise findings from the the UK-specific case to a more widely applicable tool, the results will be expressed in terms of standard statistical distributions, where the behaviour of the parameters specifying the distributions are analysed as the degree of aggregation is increased.

2. Methodology

The main approach was to use sets of hourly wind speed data, convert these to corresponding hourly power output time series, and then combine them to an aggregated power output time series. The characteristics of each of these time series was then summarised in the form of histograms normalised to probability density functions. These analysis steps were first applied to observed wind speed data. To generalise the results, the analysis was then applied to ensembles of randomly generated Weibull-distributed wind speeds. An ensemble consisted of either independent samples or cross-correlated samples to mimic the spatial correlation of observed wind speeds.

This section will first describe and justify the choice of wind speed observations in §2.1 and the standard Weibull distribution used to generate the surrogate data in §2.2. Section 2.3 then describes how wind speed was converted to wind power, followed by an introduction to the beta distribution which was used to describe the statistics of the resulting power output in §2.4.

Finally, Sections 2.5 and 2.6 describe how the power output time series from the observed and randomly wind speeds were aggregated to combined power contribution to the grid.

2.1. Wind speed data source for observed distributions

From the options outlined by Watson et. al [37], the approach to use wind measurements from land stations was adopted. From an larger set of possible sites, the 72 sites indicated in Figure 2 were chosen to provide a representative coverage of the available area as well as a good distribution of distances between pairs of sites and which, at the same time, covered the two-year period from 1 January 2012 to 31 December 2013 with more than 98% of valid data for each site. The data were supplied through the British Atmospheric Data Centre (BADC) from the UK Met. Office Integrated Data Archive System (MIDAS) [36], with the details for each station listed in Appendix A. The MIDAS stations provide hourly readings of the wind speed from anemometers at a nominal height of 10 m above ground, rounded to the nearest *knot* (1 kn = 0.5144 m/s).

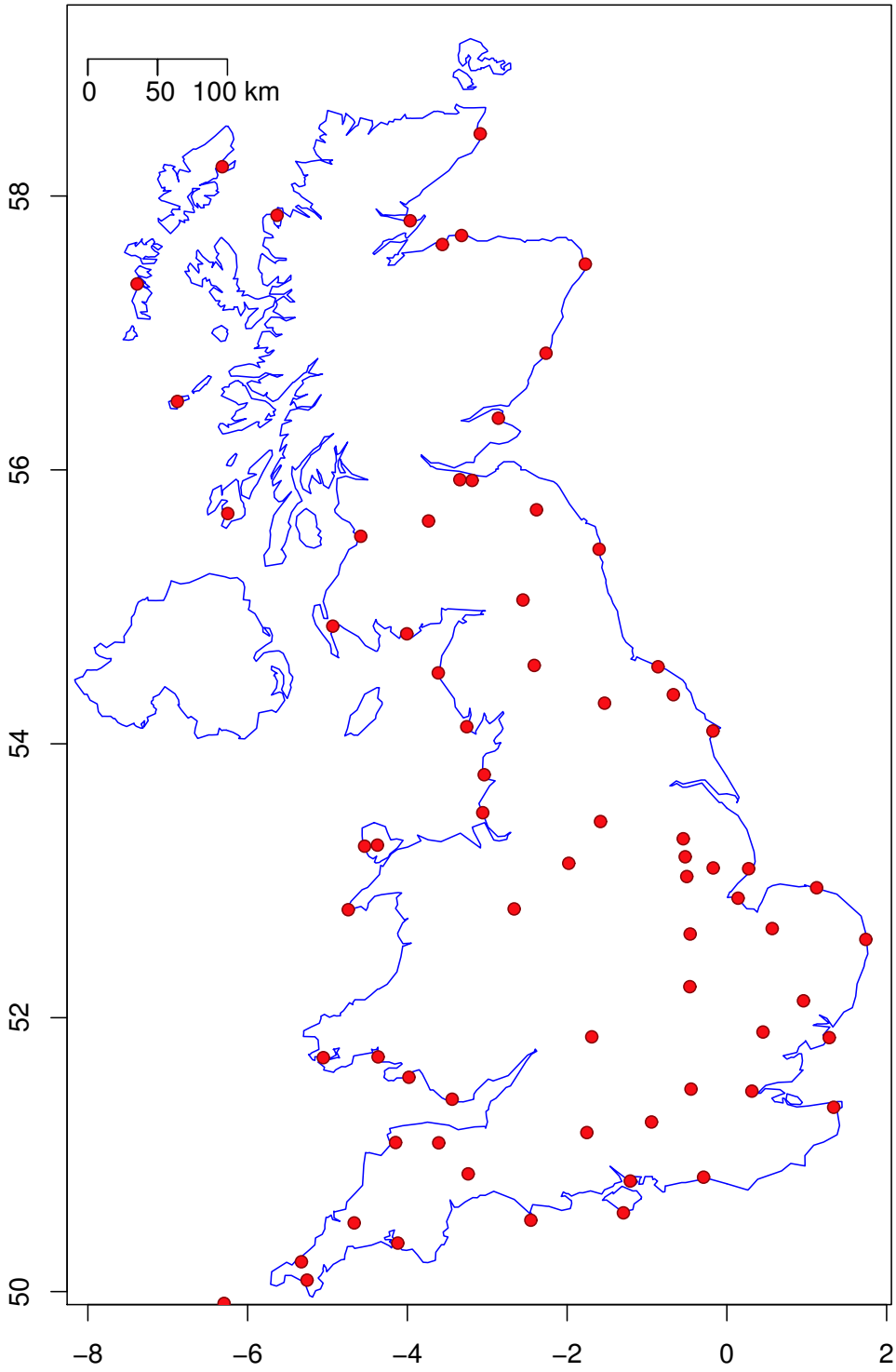

Figure 2. Map of the UK showing the location of the 72 sites of wind speed measurements. Station details are listed in Appendix A.

2.2. Standard wind distribution used

The wind speed measurements from the observations were used directly to calculate the power for individual sites and their aggregation. To generalise the results, a standard distribution was used to generate surrogate wind speed samples. The Weibull distribution,

$$f_W(u;c,k) = \frac{k}{c}\ \left(\frac{u}{c}\right)^{k-1}\ e^{-\left(\frac{u}{c}\right)^{k}}, \tag{1}$$

describes the frequency or probability of a particular wind speed u in a distribution with a scale factor c (in units of wind speed) and a shape factor k. The Weibull distribution is known to be a good representation of actual distributions in mid-latitudes and is frequently used. The scale factor, c, is closely linked to the location of the peak of the distribution and the mean wind speed. The shape factor describes how narrow or broad the distribution is, with typical values of $1.7 \lesssim k \lesssim 2$ for many mid-latitude locations. The mean wind speed for a Weibull-distributed resource is $\overline{u} = c\Gamma(1 + 1/k)$ where Γ is the gamma function. For the typical range of k this means that c is around 11% to 13% larger than the mean wind speed. The observations at all 72 sites were tested against the Weibull distribution, and each could be fitted with a goodness of fit of $r^2 > 0.92$. The results of this fitting is shown in appendix A.

2.3. Wind power estimation

For the analysis of the effect of wind speed fluctuations on the fluctuations of wind power provision to the national transmission grid, it was necessary to estimate reasonable power output levels from each region based on the local wind speed measurement.

This followed a standard procedure, e.g. [15], illustrated in Figure 3 using the data from the site with ID 858 in appendix A: the wind speed measured at the nominal anemometer height of $z_R = 10$ m was converted to m/s and extrapolated to a nominal hub height of $z_H = 80$ m above ground using a logarithmic wind shear profile,

$$u_H = U_R \frac{\log z_H/z_0}{\log z_R/z_0}, \tag{2}$$

with a surface roughness of $z_0 = 30$ mm. Figure 3.a shows the Weibull distribution for the 10 m wind speed time series as the blue line and that for the height-adjusted wind speed time series as the green dotted line. The chosen roughness length of 30 mm, also used by [37], is appropriate for short grass, which is a typical environment for a rural meteorological station.

The hourly wind speed data were then converted to hourly time series of power output through a generic turbine performance curve, shown in Figure 3.b, characterised by a cut-in wind speed of 4 m/s, a cut-out wind speed of 25 m/s, and a rated wind speed of 12 m/s at which the turbine reached its rated output. The rated power was taken as unity so that the capacity factor for that turbine, wind farm or fleet of wind farms is equal to the mean output over the analysis period. The histogram of the resulting power output time series is shown in Figure 3.c which is qualitatively identical to that constructed from actual power output data from the wind turbine in Figure 1.b.

2.4. The beta distribution

Given that the power output profile is limited to the closed interval $[0, 1]$, it is possible to approximate the observed distributions by a suitable standard distribution. In common with several authors, e.g.[4, 12, 23], the beta distribution was found to give consistently the best fit from a range of possible standard distributions. A less common 'versatile distribution' has been proposed as superior to the beta distribution for wind power [39] but this was not tested here as the goodness of fit with the standard beta distribution, carried out using the distribution fitting routine provided through R [1, 20], was very high. The probability density function of the beta distribution is

$$\phi_\beta\left(\Pi\right) = \frac{1}{B(\beta_1,\beta_2)}\ \Pi^{\beta_1-1}\ \left(1-\Pi\right)^{\beta_2-1}, \tag{3}$$

where

$$B(\beta_1,\beta_2) = \frac{\Gamma(\beta_1)\Gamma(\beta_2)}{\Gamma(\beta_1+\beta_2)} = \int_0^1 t^{\beta_1-1}\ \left(1-t\right)^{\beta_2-1} dt$$

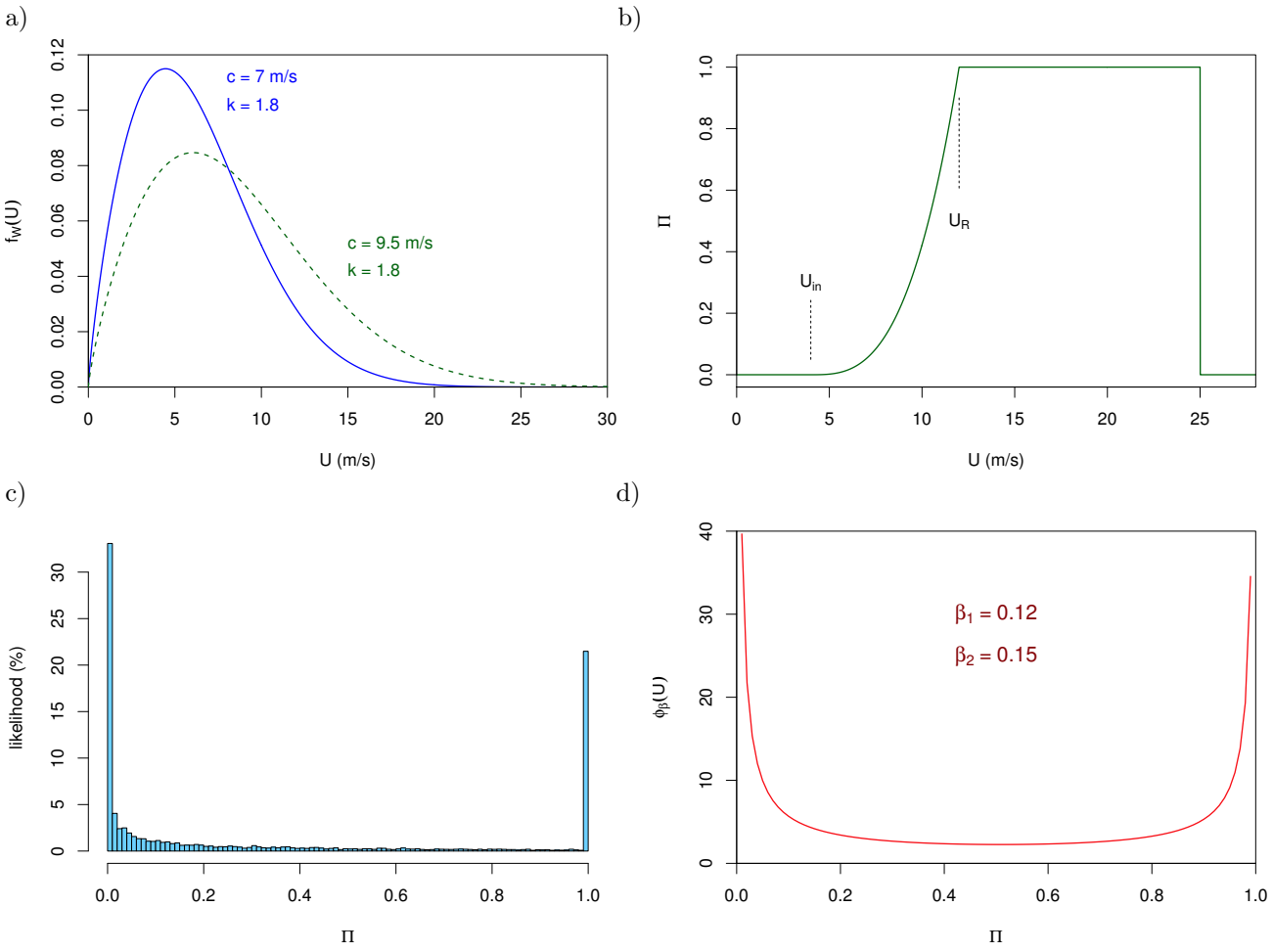

Figure 3. Procedure of converting from measured or randomly generated wind speed distribution to estimated power output distribution: a) the measured wind speed distribution is scaled from the anemometer height of 10 m to reference turbine hub height of 80 m (in the case of randomly generated wind speeds a Weibull curve was generated to represent directly the wind speed resource at hub height), b) the typical performance curve of a wind turbine to convert wind speed to power, c) resulting wind power distribution, d) best-fit beta distribution to idealise the calculated power output histogram.

is the beta function required here to normalise the distribution. The two parameters β_1 and β_2 determine the shape of this distribution such that it has a single maximum within the interval if both parameters are larger than 1, while it diverges to infinity at one or both ends if one or both parameters are less than 1. If $\beta_1 = \beta_2$, the distribution is symmetric around the centre value, $\Pi = 0.5$, whereas the maximum is shifted to lower values if $\beta_2 > \beta_1 > 1$. The mean value is $\mu = \beta_1/(\beta_1 + \beta_2)$ and its variance is $\sigma^2 = \beta_1\beta_2/\left[(\beta_1 + \beta_2)^2\,(\beta_1 + \beta_2 + 1)\right]$ [23].

The distribution-fitting routine provided by R takes as input the power output time series. However, as ϕ_β diverges at $\Pi = 0$ or $\Pi = 1$ for $\beta_1, \beta_2 < 1$, the distribution fitting function provided by R could not accept values equal to zero or 1. For that reason, all zero power instances were changed to 10^{-6} and all unit values were changed to $1 - 10^{-6}$. Applying this fitting routine to the power output time series for the example in figure 3 results in the two shape parameters $\beta_1 = 0.12$ and $\beta_2 = 0.15$ with that beta function plotted in Figure 3.d.

2.5. Aggregation of UK sites

The aggregated power by combining a subset of the full 72 stations was created by taking a random sample of size $N_s < 72$, and averaging the power output over those N_s sites for each point in time. The averaging performs the same function as adding the power and then dividing by the installed capacity of individual sites, as our analysis was restricted to unit capacity at each site. This sampling was repeated a number of times to create a random representation of aggregating different sites. Because sampling the finite set of stations too many times would result in sampling the same combination of sites again and again, it was important to have a large enough sample to represent typical statistics but small enough to avoid oversampling the population. Trial and error suggested that sampling at least 20 times was sufficient to result in a repeatable spread of results but that one should not sample more than 35 times. All results presented below are based on a repeating the sampling 30 times.

In addition to the random sample, we also explored a sequential sampling of incrementally adding neighbouring sites, and thereby gradually increasing the spatial extent of the wind power cooperative. One of these sequences started with the most northern site and extended southwards, another started with the southern most, and a third started in the centre of the UK and extended outwards.

2.6. Aggregation of Weibull sites

As one objective was to assess the effect of spatial cross-correlation of the resource, both fully independent and partially correlated wind speed distributions were generated and then aggregated.

Initially, for the aggregation of up to N_s independent Weibull sites, N_r realisations of N_s sets of Wind speed samples were generated, where each sample contained two years' worth of hourly (17544) wind speed measurements. The wind speeds were then converted to wind power, following §2.3, and then this power output was aggregated for the N_s sites for each hour in the year.

After some testing, it was found that a reliable procedure to produce random yet cross-correlated wind speed distributions was to generate one random Weibull-distributed reference wind speed sample, $u_R(t)$, and N_c independently generated Weibull-distributed wind speed samples, $u_{r,i}(t)$, for the $i = 1 \ldots N_c$ sites. To achieve a cross-correlation consistent with the observations, each site-specific sample was then combined with the reference wind speed sample as

$$u_i(t) = c_r u_R(t) + (1 - c_r)\, u_{r,i}(t) \tag{4}$$

with

$$c_r = \frac{1}{\pi} \arccos\left(1 - 2r\right) \tag{5}$$

to represent sites with a Pearson's correlation coefficient of r, e.g. [24, §2.3.4].

As with the independent sites and the observations, a sample of N_s sites was taken from these now cross-correlated N_c sites to combine their output to an aggregated power output in the same way as for the observations.

3. Results from observed wind distributions

In this section, the results from the analysis of the wind speed observations from the 72 Met.Office stations are described, starting with an analysis of the signature of the cross-correlation among sites, then of the effect of aggregating the output from different sites.

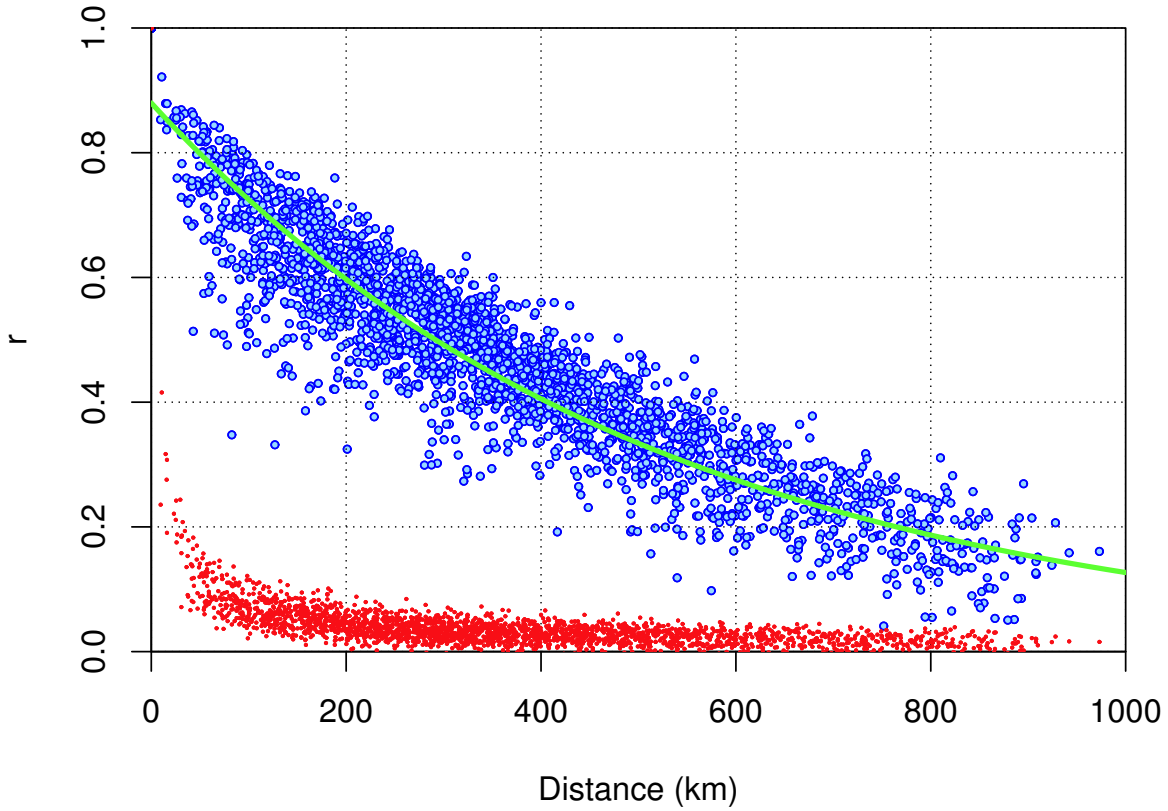

Figure 4. Cross-correlation of the wind speed data across pairs of Met.Office stations against their pairwise distance (blue circles) and, as red dots, the corresponding cross-correlation of the hour-to-hour wind speed changes.

3.1. Wind speed coherence and variability

Figure 4 compares the pairwise correlation of the hourly wind speeds (blue circles) and of the hourly wind speed changes, $\delta u/\delta t$ (red dots), against the distance between the stations. There is a clear link between the wind speed and the distance, decreasing rapidly from $r \approx 0.9$ for the closest station pair to around $r = 0.5$ at a distance of 200 - 300 km, followed by a more gradual decay to $r \approx 0.2$ at around 700 km. The wind speed fluctuations, on the other hand appear to be largely uncorrelated except for the the closest pairs with distances less than 50 km. This is clear evidence that the wind speeds over the entire UK reflect the synoptic weather patterns with spatial coherence of length scales of hundreds of kilometres. The pattern formed by the blue circles in Figure 4 for the wind speed is entirely consistent with the analysis by Sinden [30] for estimated power output at a very large number of sites across the UK as well as the correlation between sites across Germany [19]. However, Figure 4 also shows that the hourly variation is not significantly affected by the large-scale teleconnection but by much more localised events. This demonstrates on one hand that variations of the wind over a typical weather regime will affect the nationally available wind power, with implications for scheduling of other forms of generation. On the other hand it suggests, that it might be possible to smooth out short-term power fluctuations from individual wind farms by aggregating them with other wind farms across the country. The result is that implications of power quality and short-term energy storage might not be too severe an issue when integrating a substantial amount of wind power into the transmission system.

3.2. Time scales associated with spatial coherence

To explore the temporal aspect of the relationship between different locations, the correlational analysis is extended to filtered wind speed data and their residual. For a chosen filter length from 2 hours to 1 year, the wind speed time series was filtered using a moving-average for the low-pass filtered component, u_f, and

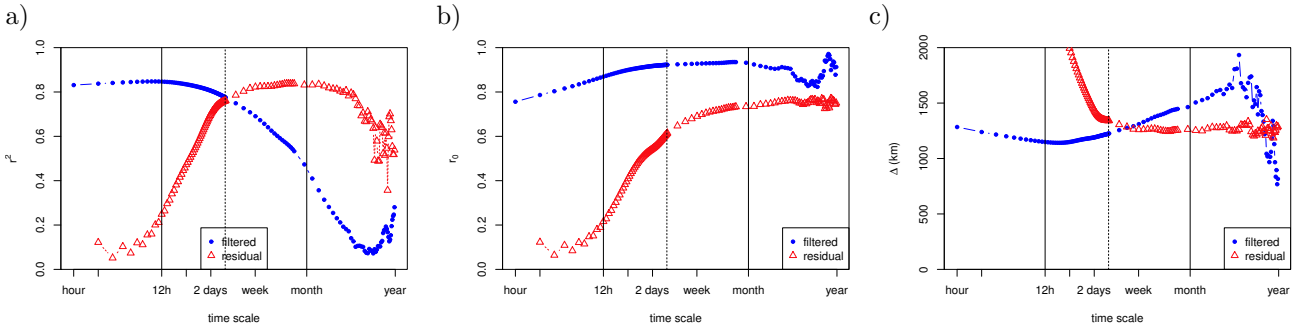

Figure 5. Change of the cross-correlation across sites with temporal low-pass filtering (blue dots) and high-pass filtering (red triangles), using moving-window averaging, against the filter window length

the residual, $u_r = u - u_f$. One observation was that the 'exponential' decay with distance in the correlation coefficient was replaced by a much more linear decay of the correlation of the low-pass filtered wind speed among pairs of sites. To quantify the degree of correlation, and the spatial decay of correlation, a linear regression of Pearson's correlation coefficient against distance between the stations was performed for all filtered and residual time series. The results of these regressions are shown in Figure 5, with the goodness of fit as a measure of consistent behaviour in Figure 5.a, the intercept as a measure of nearby correlation in Figure 5.b, and the slope as a measure of the spatial decrease in correlation among sites in Figure 5.c.

The characteristics of Figure 5 are that the low-pass time series show a very consistent behaviour as long as time scales less than around three days are included (from Figure 5.a), that the degree of correlation at close distances increases if time scales less than 12 hours are eliminated (from Figure 5.b), and that the range of the correlation is on the order of a thousand kilometres (from Figure 5.c). At time scales larger than a season, the spatial cross-correlation loses its systematic behaviour rapidly. Conversely, the high-pass filtered time series or residual is virtually uncorrelated at time scales shorter than 12 hour and reaches a point of maximum systematic behaviour as measured by r^2 in Figure 5.a when time scales less than a month are included.

These characteristics can be interpreted that the wind speed at any time can be roughly assigned to three fundamental processes:

1. At time scales less than 12 hours, localised dynamics dominate the wind speed fluctuations. This finding is in good agreement with the spectral analysis by Tarroja et al. [34] who observed a reduction in spectral density at time scales shorter than 12 hours after aggregating nearby wind farms. In fact, if the power sources being aggregated are largely uncorrelated, then the fluctuations from combining N independently fluctuating sources should scale with $N^{-1/2}$ [2]. Figure 5 therefore shows that combining wind turbines or wind farms separated by more than around 50 km will be effective at smoothing out power fluctuations at time scales up to 12 hours.
2. At time scales between 12 hours and a month (with a peak at around 3 days), the wind speed is dominated by the large-scale atmospheric dynamics including the daily cycle and synoptic weather systems which have a typical length scales of several hundred to a thousand kilometres. These are the time scales which lead to spatial correlation of the wind speeds and wind power across substantial distances. As a consequence, one can expect gains in balancing wind power for a more reliable output only if wind farms cover a very large area, such as the size of the entire UK.
3. At seasonal and annual time scales, the local time-invariant environment, such as the local topography, dominates the flow, and the wind speeds are determined by their local long-term average.

3.3. Observed local and national power

Figure 6.a shows a histogram of the individual power output calculated from the 72 sites. This figure is fully consistent with the earlier illustration from Figures 1.b and 1.c: most of the time an individual wind turbine is not producing, some of the time it is producing at rated power, and some of the time somewhere in between. Keeping the scale identical but showing the histogram for the total output over the two years shows a very different behaviour, consistent with Figure 1.d. The high degree of correspondence between Figures 1 and 6

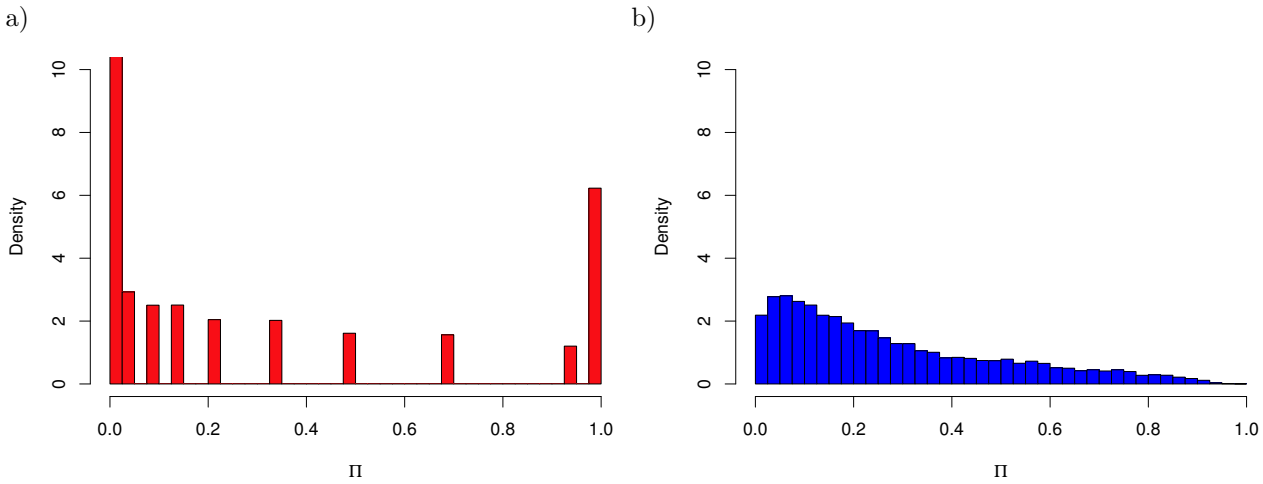

Figure 6. Histograms of power output from the observations; a) all 72 stations individually counted, b) the power from all 72 stations combined to a total power output.

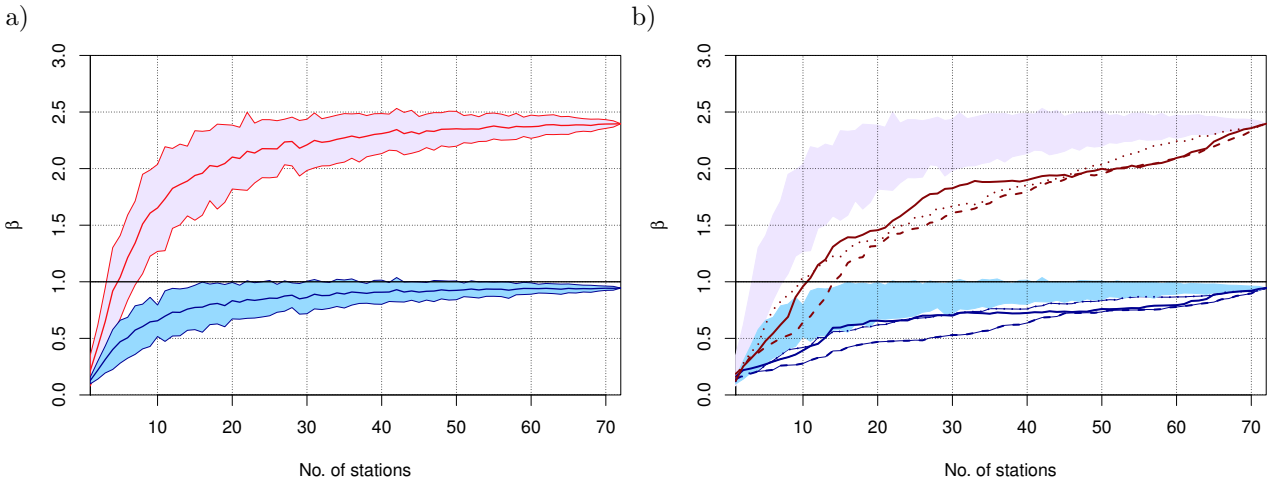

Figure 7. Beta parameters for fitting beta distributions to aggregated power output against number of sites combined from the 72 Met.Office sites; a) range of parameters for repeated random sampling and, b) parameters for incrementally adding neighbouring sites; solid line: starting in the North, dotted line: starting in the South, dashed line: starting in the centre.

provides a validation of the approach taken here of using wind speed data as proxy for wind power, and that the number of sites included and their spatial coverage are representative of the UK system studied here.

Figure 6.a clearly would be consistent with a beta distribution with both shape parameters $\beta_1 < 1$ and $\beta_2 < 1$, whereas Figure 6.b would be consistent with a beta distribution with $\beta_1 \approx 1$ (occasional but not frequent periods of no wind power) and $\beta_2 > 1$ (rare full power output). The transition from the extreme behaviour of a single turbine or farm to the much more moderate wind power profile of the national fleet is illustrated in Figure 7 of the two beta shape parameters against N_s, the number of sites combining to a single power output, where the lower (blue) region shows the range of values found for β_1 and the upper (red) region for β_2 when aggregating 30 different random samples of N_s sites. Obviously, as the sample size approaches the population size of the 72 stations, fewer different samples are possible, and the range in observed results reduces. This effect can clearly be seen from a sample size of 30 onwards. However, the general shape of the progression is very clear, with an initial rapid increase in the shape parameters until around ten to 15 sites from across the UK, followed by a much slower increase eventually reaching what appears a saturation value. In the case of the UK sample, these saturation values are $\beta_{1,sat} = 0.94$ and $\beta_{2,sat} = 2.4$. Figure 7.a shows the range and median of the shape parameters when aggregating random samples from across the UK. In contrast, Figure 7.b shows three special cases where nearest

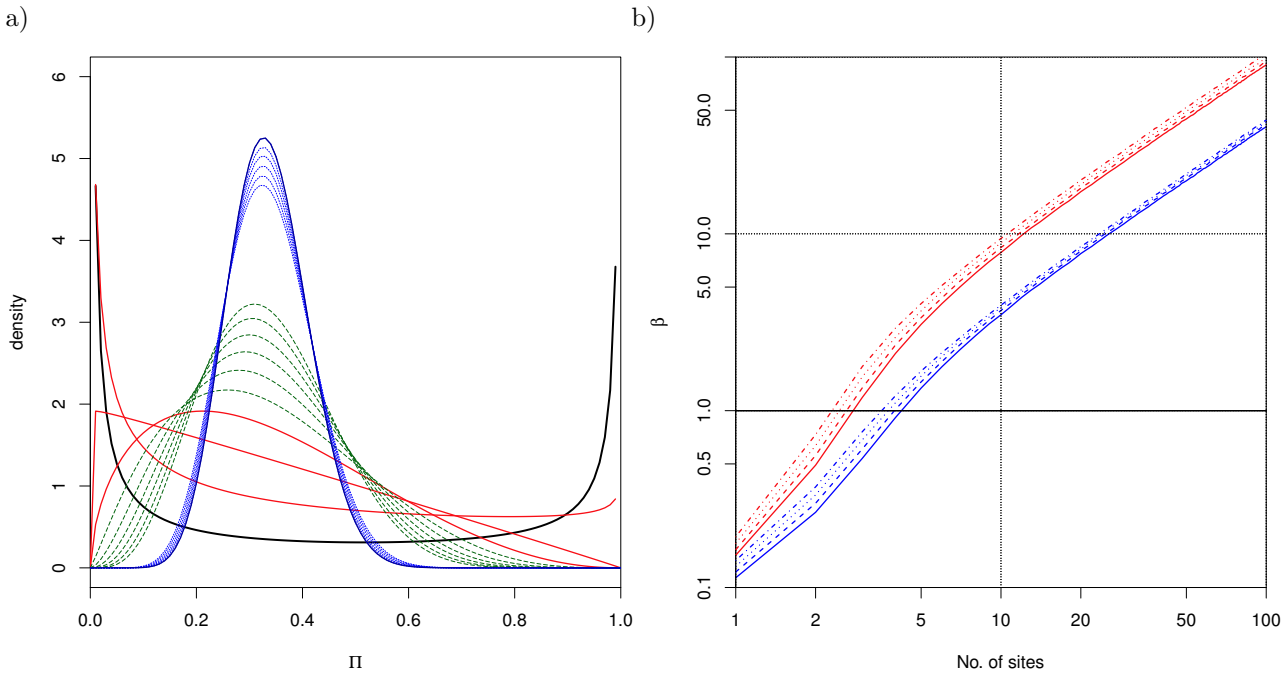

Figure 8. Illustration of aggregating the power from up to 100 independent Weibull sources; a) beta distributions representing the power from a single (black line) through a few (red solid and green dashed lines) to tens of sites all with Weibull parameters $c = 9\text{m/s}$ and $k = 1.8$; b) Change of beta shape parameters (blue for β_1 and red for β_2) against number of sites contributing, all with Weibull scale parameter $c = 9\text{m/s}$ and a range of shape parameters (solid line: $k = 1.6$, dashed: 1.8, dotted: 2, and dash-dotted: $k = 2.2$

neighbours are incrementally added to the participating sites. While they all end up at the same result when the entire available fleet is included, the incremental addition has always a slower increase in the shape parameters than the random addition. In particular, starting in the centre and combining sites outwards has the least impact but this might be partially due to the fact that the wind resource is best in the far North and far South.

4. Results from a standard wind distribution

To generalise the observations from section 3 and to develop a simple model of the effect of aggregating partially correlated generation units, we turn from the observed distribution to wind speeds generated by sampling from the standard Weibull distribution. In the first step, the effect of aggregating the power output from independent Weibull sources is demonstrated, in § 4.1. After this, the power output from partially correlated Weibull sources, created as described in § 2.6, is presented in § 4.2.

4.1. Aggregating independent Weibull sources

Figure 8.a shows the results of aggregating up to 100 independent Weibull sites, all with a scale factor of $c = 9\text{m/s}$ and a shape factor of $k = 1.8$, values typical for the mean UK wind resource. The solid black line is the beta distribution resulting for the power output from a single Weibull site, the solid red lines are for two, three, and four sites. The dashed green lines are from aggregating five to ten sources, and the dashed blue lines from 20 to 90 sources (every ten), and the final solid blue line has arisen from aggregating 100 independent sites.

While the mean power remains the same throughout, the distribution moves from the extreme 'bathtub' shape for a single site rapidly to a single-humped smooth distribution with a maximum approaching the mean value. Increasing the number of sites progressively sharpens the distribution around the mean. This behaviour is also captured by the plot of the two beta parameters shown in Figure 8.b for Weibull parameters $c = 9\text{m/s}$ and shape values between 1.8 and 2.2. After an initially faster increase, up to five sites, the beta parameters increase linearly without ever seeming to saturate for all cases.

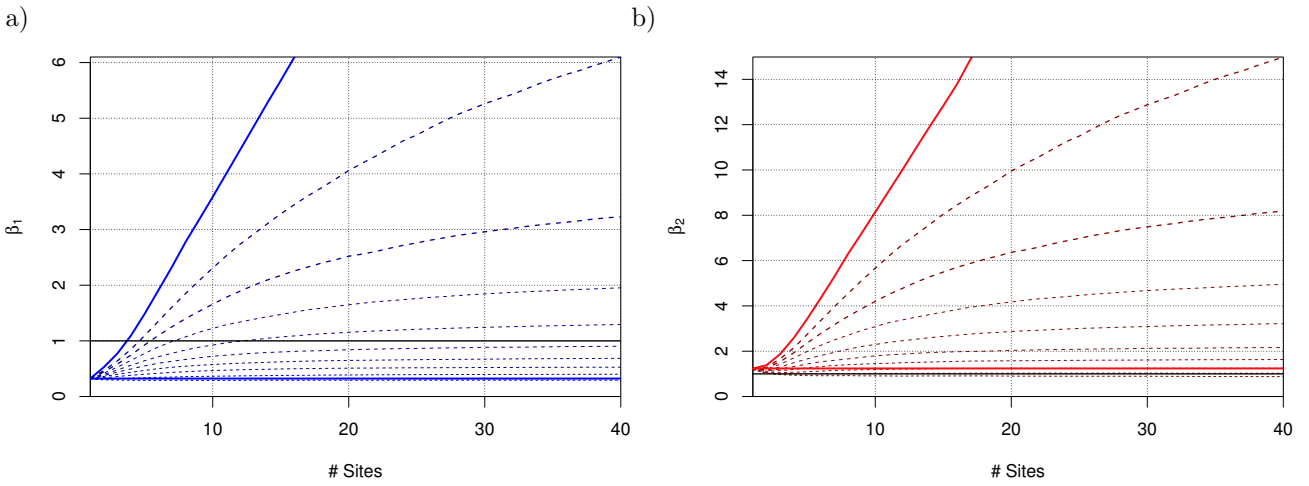

Figure 9. Change of beta parameters, a) β_1 and b) β_2, against number of sites aggregated for a selection of partially correlated Weibull sites, all with $c = 9$m/s and $k = 1.8$ with cross-correlations across the sites ranging from zero to 1 in steps of 0.1.

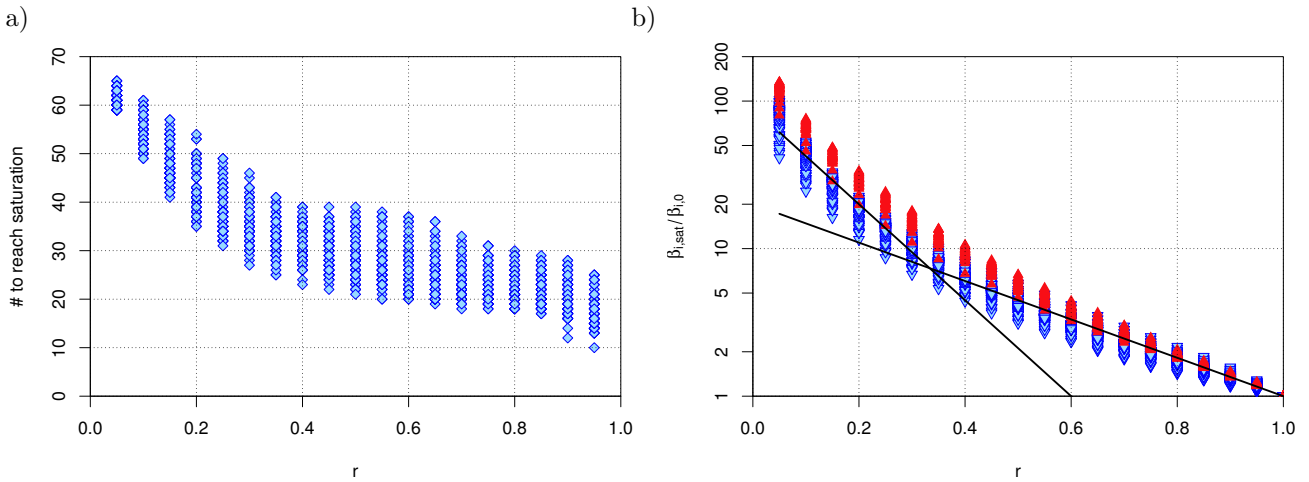

Figure 10. Change of beta parameters with correlation; a) onset of saturation, and b) saturation value as function of correlation.

4.2. Aggregating partially correlated Weibull sources

Figure 9 shows how the change in the beta parameters is affected by aggregating partially correlated sites rather than independent sites for sites with Weibull parameters $c = 9$m/s and $k = 1.8$, where Figure 9.a shows β_1 against the number of sites aggregated and Figure 9.b shows β_2. The upper solid line reproduces the result for independent sites from Figure 7.b and the lower solid line shows the case of N_s identical sites. The dashed lines in between show different cases of correlation, increasing the correlation coefficient r as used in eq. (5) from $r = 0, 0.1, 0.2, \ldots 1$. Here one can see that the effect of reducing the effectiveness of aggregating sites is significant even at the lowest correlation of $r = 0.1$, and that saturation of the benefits sets in after only a moderate number of sites, even at a moderate value of correlation across the sites.

The final part in the analysis is to evaluate at which point the saturation sets in for a given correlation across sites and what the saturation value is. This is shown in Figure 10 for a range of Weibull parameters, $c = 6.5 \ldots 12$m/s and $k = 1.6 \ldots 2.2$. In Figure 10.a one can see that the number of sites after which saturation sets in rapidly drops from 60 to 70 sites at $r = 0.05$ to between 20 and 40 for a range of $0.3 < r < 0.7$ after which it further reduces to between 10 and 20 at $r = 0.95$. For the value to which the beta parameters converge, it was found that this was most consistently described as the ratio of the final value for aggregating 100 sites over the initial value for the single site. This ratio is shown for both beta parameters in Figure 10.b with blue down-ward

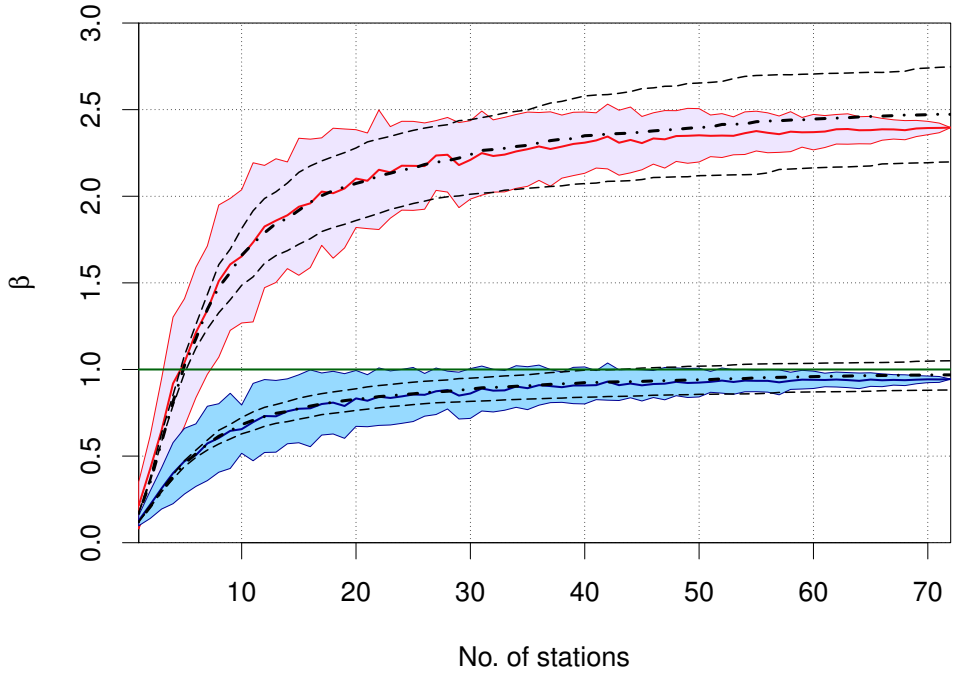

Figure 11. Comparison of the model's prediction against the results of the random aggregation of the observations. The model parameters are the mean Weibull parameters from the observations scaled up to the notional hub height and the three choices of mean cross-correlation: the median of the observations (central dash-dotted line) and the 45% and 55% quantiles (the two dashed lines).

pointing triangles for β_1 and red filled upward pointing triangles for β_2. In line with the linear increase of the parameters for independent sites, the ratio between the final and initial value is around 100 at very low correlation among sites. At the other end, identical sites do not alter the power output, and the ratio between the final and initial value is 1. For intermediate values, the ratio decays in a consistent manner. Superimposed on the results are two lines approximating that behaviour as

$$\frac{\beta_{sat}}{\beta_0} \approx 20^{\alpha} \qquad \begin{cases} \alpha = 1 - r & \text{for} \quad r >\sim 0.4 \\ \alpha = \frac{0.6-r}{0.4} & \text{for} \quad r <\sim 0.4 \end{cases} . \tag{6}$$

This figure demonstrates that is possible to estimate the power output profile based on the cross-correlation of the wind speeds between pairs of sites planning to offer a combined electricity production. The projected combined distribution can be used in the form of load duration curves to assess how reliably the aggregation of wind farms can supply electricity to the grid. Since the correlation is a clear function of the distance between sites, gains through combining near-by wind farms are very limited, whereas combining output from farms across a distance of hundreds of kilometres is very effective, even when combining only 10 to 20 wind farms.

5. Discussion

Having been able to demonstrate that short-term wind power fluctuations even from relatively closely situated wind farms are essentially independent, a consequence is that power fluctuations are normally distributed with a standard deviation scaling with the number of contributing sites, N_s, as $N_s^{-1/2}$. This can support statistical wind power forecasting, e.g. [29, 32], as well as refine models of electricity market participation of wind farm consortia, e.g. [3], or for optimising wind farm development, e.g. [22].

In section 3, Figure 7, the effect of aggregation wind speed observations from across the UK was shown. Guided by this, a simple model based on standard wind speed and wind power distributions, and the aggregation of partially correlated samples from the wind speed distribution, was developed in section 4. Figure 11 overlays

the results of this model over the observations. The model used 72 Weibull sites, all with mean Weibull parameters from the observations scaled up to the hub height of 80 m ($c = 8.82$m/s and $k = 1.81$) and using the median of the correlation coefficient among the observations (cf Figure 4) as the correlation parameter $r = 0.473$ in eq.(5) for the dash-dotted line. In addition, the values of the 45% and 55% quantiles for the correlation coefficient of $r = 0.450$ and $r = 0.493$ were used to generate the two dashed lines respectively. The extremely good agreement between the effect of randomly aggregating the power from the observation sites with the simple model, only requiring a mean wind resource estimate and a mean spatial cross-correlation coefficient, demonstrates that it is now possible to estimate the wind power profile of joining different generating sites where only knowledge of the local, or even national average wind resource and the distance among potential partners is needed, as the correlation among sites is mainly determined by their respective distance.

Based on the model, it is now possible to model generation duration curves used for calculating the contribution of individual generators or aggregated generators to electricity supply. This can therefore be a useful tool when planning to develop a site and, in particular, when proposing a consortium to set up, what is now called a 'Virtual Power Plant' (VPP), e.g. [5, 28, 35], as an economic tool to add reliability to wind power. This study has only considered a single form of energy resource, and the next logical step is to extend the analysis to include other resources such as PV, wave or tidal power, each with their own characteristic. There is evidence that even co-located generators from different resources, e.g. wind and solar, have very little correlation among them [6], so that the combination of different resource will quickly lead to a beneficial generation profile.

This analysis has concentrated on the wind power output only, without regard to the actual demand. Both, the daily electricity demand profile will have a strong influence on planning and contingencies required to effectively integrate wind power, e.g. as demonstrated in an idealised analysis [17], but also more generally over the year. To illustrate the effect regional aggregation of wind power can have on the residual load duration curves, the wind power from an increasing installed capacity at the 72 locations was used to contribute to the UK's national demand over the same 2-year period as the wind speed data. In that analysis [16], the effectiveness of aggregating wind power was compared against that which could be achieved by demand-side management and short-term energy storage as well as seasonal balancing of supply and demand. The scenarios investigated ranged from no and current wind power output to an installed capacity sufficient to cover the entire annual electricity consumption from the annual electricity production from these wind sites.

Figure 12 shows the residual load duration curve for a range of balancing actions when 50% of the annual electricity consumption is produced by wind power, and the remaining 50% is initially scheduled one day ahead based on expected demand wind production. The residual load is the difference between the demand at any hour in the analysis and the electricity production by wind, scheduled, and results of energy management options. The pale red region shows the ranged covered by the residual load if all the wind power is from a single site and no further action is used prior to balancing. The pale yellow region shows by how much the residual load is covered through short-term energy and power management actions which are effective on the hourly scale, such as demand-side re-scheduling of load or exporting/importing electricity to other systems. The strong yellow region indicates the residual load after the daily cycle has been managed using strategies such as energy storage or stand-by generation. The green area denotes the effect of the regional aggregation when all 72 sites combine to the wind power. Finally, the blue region is the result of combining all actions. Clearly, regional aggregation reduces the number of high residual load noticeably and it also reduces the number of residual power excess (negative residual load) drastically compared to a single site, and even compared to other energy balancing actions.

To illustrate, how the aggregation of individual wind power producers to a national wind fleet affects the requirements for other generation planning and balancing in future scenarios, Figure 13 shows the required generation capacity against wind energy contribution to meet demand. The grey triangle represents the installed capacity of the schedule generation, decreasing directly with the wind contribution from 100% to 0%, the combination of the other shaded regions indicates the total required generation capacity in addition to the schedule generation and wind power if the wind power source is from a single site. As the wind contribution increases, and the scheduled contribution decreases, the additional capacity increases steadily, though not quite as fast as the scheduled generation decreases.

The savings made through aggregating wind farms to a national wind fleet is shown by the upper hatched and shaded regions in Figure 13, while short-term demand management over a few hours does not reduce the remaining capacity requirement noticeably. Separating the daily cycle from the longer term requirements leads to the remainder being separated into three regions, where the yellow area indicates the requirement to cover the

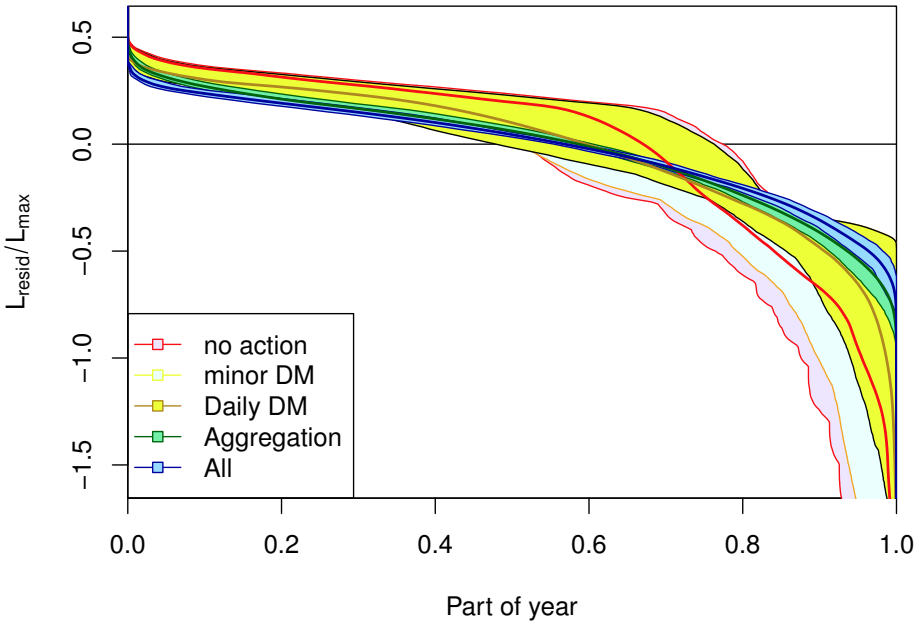

Figure 12. Residual load duration curve for the UK's national demand if 50% of the annual consumption is provided by wind and 50% by day-ahead planned scheduled generation. The regions annotated as '*minor DM*', '*Daily DM*' and '*Aggregation*' indicate the range of residual load duration curves under each of these actions separately, and only '*All*' combines these actions. '*minor DM*' refers to load-shifting, energy storage or interconnections from one hour to the next only, while '*Daily DM*' refers to load-shifting and energy storage actions acting over several hours up to the daily cycle.

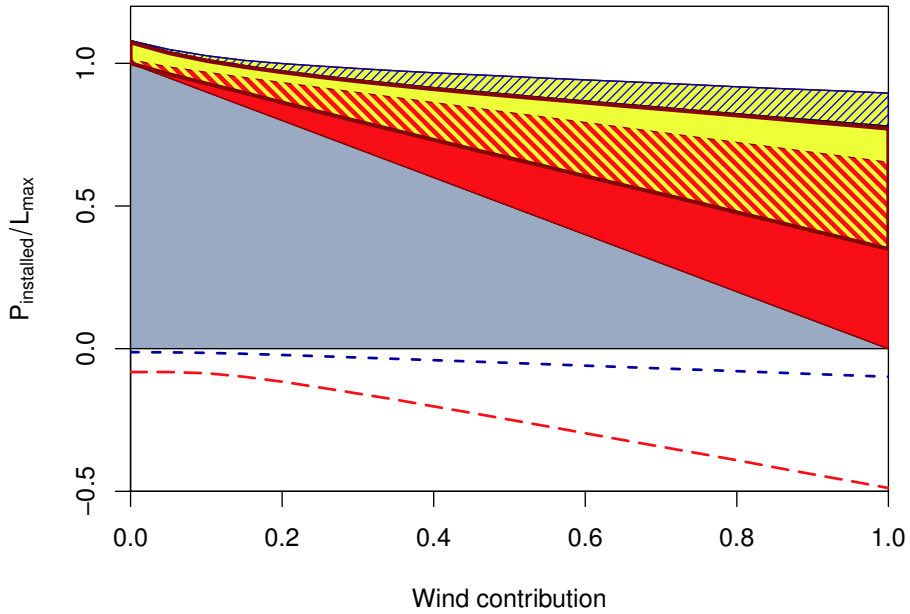

Figure 13. Required capacity to supply the residual load for 99% of the time: grey area: conventional generation scheduled a day ahead; red: required to supplement wind and scheduled generation and time scales exceeding a day; red-yellow cross-hatched: requirement to be able to respond at all time scales: yellow: requirement for short-term balancing up to the daily cycle; blue-yellow cross-hatched: balancing achieved by effective regional aggregation; blue line: power which system needs to be able to absorb at the hourly time scale; red line: power which system needs to absorb at the daily-cycle time scale.

daily cycle but not any longer-term needs. The central shaded region covers the requirements which have to cover both, the daily cycle and the longer term needs, while the red region is to supply only the electricity beyond the day ahead. This separation can be interpreted such that most energy storage technologies, which operate at the daily time scale, and extensive demand management strategies can only effectively address a restricted part of the balancing requirements. The remainder splits relatively evenly into those types of generation which have to provide power at all time scales and those which are only needed for the slower response beyond the day-ahead scheduling. Those longer time scales are mostly associated with the synoptic weather time scale of two to three weeks and the seasonal cycle in both, demand and wind resource.

The level of power to be absorbed, either by short-term demand management or by action to absorb the daily cycle are indicated by the two dashed lines in Figure 13.

The analysis shows that conventional energy storage systems, such as pumped hydro, cannot provide the substantial capacities needed to absorb excess power or provide the residual load over synoptic and seasonal time scales. The energy storage required over those time scales will be much more economic if the energy is stored in the form of a fuel, for example using the 'power-to-gas' concept, e.g. [9, 18, 38].

6. Conclusions

The analysis presented here has identified three main time scales affecting the spatial coherence of wind power:

1. 'short' time scales extending as far as 12 hours ahead where the wind at individual sites is dominated by the local fluid dynamics. The result is that power fluctuations at these time scales are virtually independent across a spatial portfolio of wind generation;
2. an 'intermediate' time scale ranging from the daily cycle up to the synoptic weather time scale of up to three weeks at most, where the synoptic weather regimes result in a clear spatial correlation of wind energy production; the correlation of the power output from stations is consistent with a linear decrease as a function of distance;
3. 'long' time scales longer than three weeks where the local geography determines the local mean wind resource.

The implication of these time scales is that the annual electricity will be proportional to both, the installed capacity and the local mean wind resource. However, as sites are virtually uncorrelated at time scales less than a few hours, short-term fluctuations should balance each other out such that the short-term power fluctuations will only be proportional to the square-root of the installed capacity if it is installed with reasonably broad spatial diversity. This will reduce the requirements for back-up generation or energy storage needed to maintain power quality and short-term energy balancing. At the intermediate range, important for day-ahead scheduling and week-ahead planning, the total wind energy and power production will strongly depend on the weather with consequent implications for relying on other forms of generation. However, as the time scales are relatively long, it should be possible to optimise the scheduling of reserve generation or energy storage if sufficiently good forecasting methods are used.

For the longer time scales from the daily to the seasonal cycle, we have developed a simple statistical model to estimate the effect on the power generation profile of combining spatially dispersed wind power sources. This model was based on generating random but partially correlated samples with given Weibull distributions and converting those to aggregated power samples using a generic turbine performance curve, which then could be presented as power distributions. The results from this model showed good agreement with the power generation profile from actual wind speed observations. The key results from this analysis are:

1. The power output profile from spatially dispersed wind power sources can be modelled in a simple statistical model only requiring information on the mean wind resource and either the mean cross-correlation among sites or the mean distance among sites.
2. Aggregating neighbouring sites has little effect and hence provides little benefit for the operator.
3. Aggregating a few spatially distributed sites over a reasonably large area (distances over 300 km) leads to substantial balancing of wind power with the results that the combined output is rarely at extremes (zero or full power) but most likely at values around the mean.
4. The added benefit through adding further sites rapidly saturates, such that the full potential of spatial balancing across distances of around 1000 km is achieved when combining 20 to 30 sites.

An immediate application of these results is for developers or operators of wind farms. As the estimator only uses the local or mean national wind resource and the mean distance among the sites to estimate the joint power output profile, it can be used by developers to form the most effective consortium and to estimate the reliability of their joint power output.

In terms of further development, the next step is to extend the analysis to other resources, such as photovoltaics, wave energy, or tidal power. Furthermore, the results of this work can be used in modelling complete energy systems.

Acknowledgements

We would like to thank the UK Meteorological office for providing access to the wind data from the MIDAS record through the British Atmospheric Data Centre (www.badc.ac.uk) and for providing additional anemometer details.

REFERENCES

1. Adler J, (2010) *R in a nutshell*. O'Reilly: Beijing Sebastopol.
2. Albadi M H, El-Saadany E F, (2010) Overview of wind power intermittency impacts on power systems. *Electric Power Systems Research*, 80(6):627–632.
3. Baeyens E, Bitar E Y, Khargonekar P P, Poolla K, (2013) Coalitional aggregation of wind power. *IEEE Transactions on Power Systems*, 28(4):3774–3784.
4. Bludszuweit H, Dominguez-Navarro J A, Llombart A, (2008) Statistical analysis of wind power forecast error. *IEEE Transactions on Power Systems*, 23(3):983–991.
5. Chalkiadakis G, Robu V, Kota R, Rogers A, Jennings N R, (2011) Cooperatives of distributed energy resources for efficient virtual power plants. In: *The Tenth International Conference on Autonomous Agents and Multiagent Systems (AAMAS-2011)*, 2: 787 – 794.
6. Coker P, Barlow J, Cockerill T, Shipworth D, (2013) Measuring significant variability characteristics: An assessment of three UK renewables. *Renewable Energy*, 53:111–120.
7. Cradden L C, Harrison G P, Chick J P, (2012) Will climate change impact on wind power development in the UK? *Climatic Change*, 115(3-4):837–852.
8. Davy T, Woods M, Russell C, Coppin P, (2010) Statistical downscaling of wind variability from meteorological fields. *Boundary-Layer Meteorology*, 135:161–175.
9. de Boer H S, Grond L, Moll H, Benders R, (2014) The application of power-to-gas, pumped hydro storage and compressed air energy storage in an electricity system at different wind power penetration levels. *Energy*, 72(0):360 – 370.
10. DECC, (2012) Electricity generation costs. Technical report, UK Department of Energy and Climate Change, October 2012.
11. Earl N, Dorling S, Hewston R , von Glasow R, (2013) 1980-2010 variability in UK surface wind climate. *Journal of Climate*, 26(4):1172–1191.
12. Fabbri A, Gomez T, Roman S, Abbad J R, Quezada V H M, (2005) Assessment of the cost associated with wind generation prediction errors in a liberalized electricity market. *IEEE Transactions on Power Systems Transactions on Power Systems*, 20(3):1440–1446.
13. Fertig E, Apt J, Jaramillo P, Katzenstein W, (2012) The effect of long-distance interconnection on wind power variability. *Environmental Research Letters*, 7(3): 034017.
14. Foley A M, Leahy P G, Marvuglia A, and McKeogh A J, (2012) Current methods and advances in forecasting of wind power generation. *Renewable Energy*, 37:1 – 8.
15. Früh W-G, (2013) Long-term wind resource and uncertainty estimation using wind records from Scotland as example. *Renewable Energy*, 50:1014 – 1026.
16. Früh W-G, (2014) How much can regional aggregation of wind farms and smart grid demand management facilitate wind energy integration? In: *Proceedings of the World Renewable Energy Congress-XIII "Renewable Energy in the Service of Mankind", 3-8 August, 2014, London, UK*.

17. Früh W-G, (2013) Energy storage requirements to match wind generation and demand applied to the UK network. In: *International Conference on Renewable Energies and Power Quality (ICREPQ'13), Renewable Energy and Power Quality Journal* 11.

18. Gahleitner G, (2013) Hydrogen from renewable electricity: An international review of power-to-gas pilot plants for stationary applications. *International Journal of Hydrogen Energy*, 38(5):2039 – 2061.

19. Hasche B, (2010) General statistics of geographically dispersed wind power. *Wind Energy*, 13(8):773–784.

20. Hornik K, (2011) The R FAQ. ISBN 3-900051-08-9. Available at http://CRAN.R-project.org/doc/FAQ/R-FAQ.html

21. Katzenstein W, Fertig E, Apt J, (2010) The variability of interconnected wind plants. *Energy Policy*, 38(8):4400 – 4410.

22. Liu S, Jian J, Wang Y, Liang J, (2013) A robust optimization approach to wind farm diversification. *International Journal of Electrical Power & Energy Systems*, 53:409–415.

23. Liu X, (2011) Impact of beta-distributed wind power on economic load dispatch. *Electric Power Components and Systems*, 39(8):768–779.

24. Marques de Sá J P, editor, (2007) *Applied Statistics Using SPSS, STATISTICA, MATLAB and R.* Springer-Verlag: Berlin Heidelberg New York.

25. National Grid, (2013) Electricity ten year statement (ETYS). Technical report, National Grid.

26. National Grid, (2013) Half-hourly demand data. Available from http://www2.nationalgrid.com/UK/Industry-information/Electricity-transmission-operational-data

27. Nolan P, Lynch P, McGrath R, Semmler T, Wang S, (2012) Simulating climate change and its effects on the wind energy resource of Ireland. *Wind Energy*, 15:593 – 608.

28. Pandžić H, Morales J M, Conejo A J, Kuzle I, (2013) Offering model for a virtual power plant based on stochastic programming. *Applied Energy*, 105(0):282 – 292.

29. Pritchard G, (2011) Short-term variations in wind power: some quantile-type models for probabilistic forecasting. *Wind Energy*, 14(2):255–269.

30. Sinden G, (2007) Characteristics of the UK wind resource: Long-term patterns and relationship to electricity demand. *Energy Policy*, 35(1):112 – 127.

31. Skittides C, Früh W-G, (2013) Wind speed forecasting using singular systems analysis. In: *International Conference on Renewable Energies and Power Quality (ICREPQ'13), Renewable Energy and Power Quality Journal* 11.

32. Sturt A, Strbac G, (2011) Time series modelling of power output for large-scale wind fleets. *Wind Energy*, 14(8):953–966.

33. Tapiador F J, (2009) Assessment of renewable energy potential through satellite data and numerical models. *Energy & Environmental Science*, 2(11):1142–1161.

34. Tarroja B, Mueller F, Eichman J D, Brouwer J, Samuelsen S, (2011) Spatial and temporal analysis of electric wind generation intermittency and dynamics. *Renewable Energy*, 36(12):3424–3432.

35. Tascikaraoglu A, Erdinc O, Uzunoglu M, Karakas A, (1014) An adaptive load dispatching and forecasting strategy for a virtual power plant including renewable energy conversion units. *Applied Energy*, 119(0):445 – 453.

36. UK Meteorological Office, (2011) MIDAS Land Surface Stations data (1853-current). NCAS British Atmospheric Data Centre. Available from http://badc.nerc.ac.uk/view/badc.nerc.ac.uk_ATOM_dataent_ukmo-midas.

37. Watson S J, Kritharas P, Hodgson G J, (2015) Wind speed variability across the UK between 1957 and 2011. *Wind Energy*, 18(1): 21 – 42.

38. Zhang G, Wan X, (2014) A wind-hydrogen energy storage system model for massive wind energy curtailment. *International Journal of Hydrogen Energy*, 39(3):1243–1252.

39. Zhang Z-S, Sun Y-Z, Gao D W, Lin J, Cheng L, (2013) A versatile probability distribution model for wind power forecast errors and its application in economic dispatch. *IEEE Transactions on Power Systems Transactions on Power Systems*, 28(3):3114–3125.

A. Weather stations list

This table summarises the 72 stations used in the analysis, listed in order from North to South. The 'ID' is its MIDAS station ID [36], the co-ordinates of the station given in 'Northing' and 'Eastings'(units *metres*) and the elevation above sea level (also in *metres*). The column 'Data av.' gives the percentage of valid wind speed readings through the 2-year period. The final three columns give the local wind resource in terms of the Weibull scale factor, c (in *knots*) at the anemometer height of 10 m above ground and the shape factor, k, together with r^2 as a measure of goodness of fit of the observed distribution to the Weibull distribution.

ID	Northing	Eastings	Elevation	Data av.	c (kn)	k	r^2
32	952230	336490	36	100	12.79	1.79	0.977
54	933097	146438	15	100	14.09	1.90	0.991
52	891274	184581	11	99.9	11.18	1.62	0.982
79	882720	283272	4	99.9	10.93	1.81	0.986
137	869822	321249	7	100	11.54	1.87	0.987
132	862804	306774	5	100	10.39	1.75	0.986
170	845826	413628	15	100	11.67	1.84	0.982
18903	842501	76319	4	99.5	16.91	2.04	0.991
177	773416	383879	134	100	14.11	1.85	0.974
18974	744871	99782	9	99.2	15.96	2.09	0.992
235	720895	346862	10	100	10.83	1.71	0.987
19260	671400	316100	57	100	9.07	1.64	0.966
251	670633	325663	134	100	12.63	1.80	0.988
23417	651275	132959	17	99.5	13.78	1.90	0.989
268	646194	375917	112	99.5	9.81	1.73	0.971
987	638426	290781	245	100	12.14	1.68	0.984
1007	627653	236902	27	100	10.15	1.67	0.975
315	614178	425338	23	100	11.32	1.86	0.981
1076	572995	364675	285	99.9	12.23	1.90	0.983
1039	555535	211696	11	100	11.36	1.72	0.980
1033	547233	271033	113	100	13.62	1.91	0.986
1074	519770	373386	227	99.2	10.19	1.43	0.975
17344	519217	473585	158	99.8	13.13	1.82	0.988
1055	514806	295570	124	100	14.05	1.90	0.989
358	496725	486420	262	98.9	12.73	2.03	0.979
17314	489141	430491	33	99.1	9.21	1.72	0.987
1078	470625	317889	15	100	11.78	1.94	0.987
373	467991	519398	15	99.4	11.14	1.77	0.977
1090	431400	331600	10	100	12.54	1.98	0.986
17309	400581	329936	9	100	12.91	1.78	0.972
527	392966	427742	395	99.2	15.19	1.92	0.976
381	379866	496841	57	99.4	10.94	2.12	0.969
56486	376358	241613	60	99.4	11.94	1.67	0.981
1145	375849	230885	10	99.5	13.87	1.81	0.985
384	365272	498793	68	100	10.99	2.14	0.971
30690	358964	401343	298	99.3	10.54	1.78	0.986
16725	356981	552182	3	100	12.40	2.07	0.976

continued on next page...

ID	Northing	Eastings	Elevation	Data av.	c (kn)	k	r^2
393	356742	522449	6	99.8	10.06	1.93	0.980
386	349260	500451	63	99.8	11.93	2.05	0.980
421	343672	609860	21	99.9	13.74	2.14	0.987
395	332784	544029	3	99.9	12.40	2.13	0.979
1161	324780	215240	95	99.9	16.94	1.94	0.984
643	322106	355280	72	99.8	9.11	1.77	0.985
409	309048	573675	21	99.8	10.14	1.87	0.987
432	303700	653400	4	100	12.92	2.07	0.957
583	302621	504288	73	99.6	10.80	2.07	0.986
461	259860	504917	85	99.5	9.90	2.15	0.972
440	251410	602543	89	100	10.14	2.18	0.972
19188	224794	568711	87	99.9	9.17	1.95	0.970
504	222464	625979	5	100	12.16	2.16	0.968
692	218058	421244	210	100	11.76	2.23	0.977
1215	205536	189143	44	100	11.52	1.96	0.983
1226	204400	236544	3	99.6	13.53	1.68	0.984
1255	187051	262739	43	99.7	14.92	1.80	0.970
708	176724	507693	25	98.9	9.13	2.03	0.981
16588	176481	560654	3	99.3	9.25	2.07	0.987
19206	168365	299883	49	99.2	10.73	1.96	0.983
775	166108	632370	49	100	11.61	2.14	0.965
862	149401	473748	118	100	10.19	1.94	0.984
889	140312	417258	126	100	10.57	2.02	0.985
1346	134401	249625	6	99.4	11.64	1.83	0.987
1285	133182	287408	348	99.6	10.71	1.99	0.988
1383	107480	312815	252	99.9	9.56	2.01	0.981
795	105461	520262	2	99	10.58	1.82	0.985
858	101246	455698	9	100	13.46	1.81	0.978
876	75338	449880	20	100	12.98	1.84	0.979
1415	70327	210977	200	99.9	11.27	2.03	0.985
1319	69251	367798	52	100	15.89	2.15	0.991
1336	52710	249216	50	99.8	11.31	1.70	0.988
1395	40678	162721	87	100	11.44	1.99	0.976
1393	25560	167096	76	99.9	12.15	2.12	0.924
1386	10456	91729	31	99.3	16.09	2.14	0.987